Available online at www.sciencedirect.com
ScienceDirect
Icarus 185 (2006) 443–456
ICARUS
www.elsevier.com/locate/icarus

Mapping of Titan: Results from the first Titan radar passes

E.R. Stofan [a,*], J.I. Lunine [b,c], R. Lopes [d], F. Paganelli [d], R.D. Lorenz [c], C.A. Wood [e], R. Kirk [f], S. Wall [d], C. Elachi [d], L.A. Soderblom [f], S. Ostro [d], M. Janssen [d], J. Radebaugh [c], L. Wye [g], H. Zebker [g], Y. Anderson [d], M. Allison [h], R. Boehmer [d], P. Callahan [d], P. Encrenaz [i], E. Flamini [j], G. Francescetti [k], Y. Gim [d], G. Hamilton [d], S. Hensley [d], W.T.K. Johnson [d], K. Kelleher [d], D. Muhleman [l], G. Picardi [m], F. Posa [n], L. Roth [d], R. Seu [m], S. Shaffer [d], B. Stiles [d], S. Vetrella [k], R. West [d]

[a] *Proxemy Research, P.O. Box 338, Rectortown, VA 20140, USA*
[b] *Istituto di Fisica dello Spazio Interplanetario, Via del Fosso del Cavaliere, 00133 Rome, Italy*
[c] *Lunar and Planetary Laboratory, University of Arizona, Tucson, AZ 85721, USA*
[d] *Jet Propulsion Laboratory, California Institute of Technology, Pasadena, CA 91109, USA*
[e] *Planetary Science Institute, 1700 E. Ft. Lowell, Suite 106, Tucson, AZ 85719-2395, USA*
[f] *U.S. Geological Survey, 2255 N. Gemini Drive, Flagstaff, AZ 86001, USA*
[g] *Department of Geophysics, Stanford University, 360 Mitchell, Stanford, CA 94305, USA*
[h] *NASA/Goddard Institute for Space Studies, 2880 Broadway, New York, NY 10025, USA*
[i] *L'Observatoire de Paris, DEMIRM 61, avenue de l'Observatoire, 75014 Paris, France*
[j] *Agenzia Spaziale Italiana, Viale Liegi 26, 00198 Rome, Italy*
[k] *Department of Electronic Engineering, University of Napoli, Via Claudio 21, 80125 Napoli, Italy*
[l] *California Institute of Technology, Geological and Planetary Sciences, Pasadena, CA 91125, USA*
[m] *Radar and Remote Sensing, Info-Com Department, University of Rome, La Sapienza, Via Eudossiana 18, 00184 Rome, Italy*
[n] *INFM and Dipartimento Interateneo di Fisica, Politecnico di Bari, 70126 Bari, Italy*

Received 25 April 2006; revised 18 July 2006

Available online 27 September 2006

Abstract

The first two swaths collected by Cassini's Titan Radar Mapper were obtained in October of 2004 (Ta) and February of 2005 (T3). The Ta swath provides evidence for cryovolcanic processes, the possible occurrence of fluvial channels and lakes, and some tectonic activity. The T3 swath has extensive areas of dunes and two large impact craters. We interpret the brightness variations in much of the swaths to result from roughness variations caused by fracturing and erosion of Titan's icy surface, with additional contributions from a combination of volume scattering and compositional variations. Despite the small amount of Titan mapped to date, the significant differences between the terrains of the two swaths suggest that Titan is geologically complex. The overall scarcity of impact craters provides evidence that the surface imaged to date is relatively young, with resurfacing by cryovolcanism, fluvial erosion, aeolian erosion, and likely atmospheric deposition of materials. Future radar swaths will help to further define the nature of and extent to which internal and external processes have shaped Titan's surface.

Keywords: Titan; Geological processes; Saturn, satellites; Satellites, surfaces

* Corresponding author. Fax: +1 540 364 1071.
E-mail address: ellen@proxemy.com (E.R. Stofan).

0019-1035/$ – see front matter
doi:10.1016/j.icarus.2006.07.015

1. Introduction

Prior to Cassini, it had been speculated that Titan might be cryovolcanically active (Lorenz, 1996; Lorenz and Mitton, 2002), have large bodies of liquid hydrocarbons (Lunine et al., 1983), or an impact crater covered surface (Muhleman et al., 1990; Lorenz, 1997). The Cassini Titan Radar Mapper has mapped a very small portion (∼6% over four swaths) of the surface of Titan, yet has already revealed a geologically young and complex surface (Elachi et al., 2005, 2006). The ability of the radar to penetrate Titan's clouds and produce high resolution (∼300 m–1.5 km, Table 1) synthetic aperture radar (SAR) images of the surface is providing a unique dataset with which to study Titan's geology. Mapping and analysis of the radar data will answer fundamental questions about Titan, in particular, the age of the surface and the nature of processes responsible for resurfacing.

Mapping provides insight into the compositional and structural nature of a planetary surface, and thereby constrains the geologic processes that have affected the surface in time and space. Standard techniques have been developed for producing planetary geologic maps from remote sensing data (e.g., Wilhelms, 1972, 1990). However, radar data of planetary surfaces produces a challenge to geologic mapping (e.g., Ford et al., 1993; Hansen, 2000). For example, geologic units will only be visible if they have backscatter characteristics distinctly different from the surrounding units, which is not likely to always be the case in plains regions or lava flow fields. Therefore, younger and older units of similar backscatter may be mistakenly incorporated into a single unit. If the surface properties of a unit change laterally, potentially its radar signature can also change, and it may be mapped incorrectly as two or more units. In addition, structures tend to be more readily identified if they are oriented perpendicular to the radar look-direction (e.g., Stofan et al., 1989). Despite these difficulties, useful geologic maps of geologically complex regions on Venus have been produced using Magellan SAR data (e.g., McGill, 2000; Bender et al., 2000).

SAR images of Titan provide even further challenges to geologic mapping than radar data of other remote surfaces because it is an icy body with complex and unusual hydrocarbon materials at the surface. Largely because the SAR is a single-polarization instrument, we do not fully understand the relative contributions to SAR brightness in the Titan radar images from surface roughness, surface topography, material composition, and volume scattering. The radiometry data obtained by the radar indicates that volume scattering does contribute to the radar backscatter, particularly in radar-bright regions (Janssen et al., 2004). Therefore, the Titan maps we have produced are radar properties maps (Figs. 2 and 3), more similar to geomorphologic maps than geologic maps in the sense that the units in these maps are not classified as true geologic or rock stratigraphic units, with a few exceptions noted below. Despite these caveats, mapping of the initial radar data returned by the Cassini Radar instrument has provided significant insight into the processes affecting the surface and is a crucial tool for the interpretation of other Orbiter remote sensing data of Titan.

Table 1
Swath characteristics

	Ta	T3
Resolution range, km	0.3–1.7	0.3–1.5
Acquisition date	26-10-04	15-02-05
Swath length, km	4500	6236
Latitude range	32–53° N	3° S–22.5° N
Longitude range	130–10° W	0.4–133° W
Incidence angle range	2–46°	2–30°

2. Description of the radar

The Cassini Radar is a K_u-band (wavelength = 2.17 cm) linearly polarized instrument operating over a wide range of geometries and conditions in four modes (Elachi et al., 1991, 2005). The Synthetic Aperture Radar (SAR) mode returns data at the highest-resolution (∼400 m), while scatterometry, altimetry and radiometry modes provide lower-resolution data. SAR data were obtained by the radar instrument on four flybys of Titan by the Cassini Orbiter: Ta (October 2004; Elachi et al., 2005), T3 (February 2005; Elachi et al., 2006), T7 (September 2005) and T8 (October 2005) flybys (Fig. 1, locations of swaths on map or globe, Table 1). The four swaths combined cover approximately 6% of Titan's surface, with swath widths of 120 to >450 km, and lengths of 4500 and 6236 km (Table 1). The T7 and T8 radar swaths were obtained in September and October 2005, and are discussed elsewhere (Lunine et al., in preparation).

At the point of closest approach, the radar beams move across the surface most quickly and the number of independent looks for each pixel is about three, which leads to higher speckle noise in the image (Elachi, 1987). As altitude increases, the speed of the radar beams across the surface diminishes and the number of independent looks per pixel increases to 20 or more. Thus, the speckle becomes progressively less noticeable as altitude increases and useful image detail is obtained even as the thermal signal-to-noise ratio falls to unity. During the Ta SAR pass, the spatial resolution varied from 300 m at the point of closest approach up to 1.7 km at the end at approximately 4000 km altitude. In the T3 SAR swath, the spatial resolution varied between 300 and 900 m below 4000 km altitude, and then up to 1.5 km at 5000 km altitude. Two noticeable instrument artifacts exist in the T3 swath (Fig. 3). First, at both ends of the swath the spacecraft abruptly changed attitude as it moved to the nadir position for altimetry data collection, and the SAR data degraded rapidly as the attitude changed. Second, the easternmost end of the SAR swath contains a data gap, where spacecraft activity during data downlink caused the telemetry system to momentarily lose contact. The gap is irregular in shape due to the staggered antenna beams, and image data degrade gradually prior to and following the gap as multiple looks are built up.

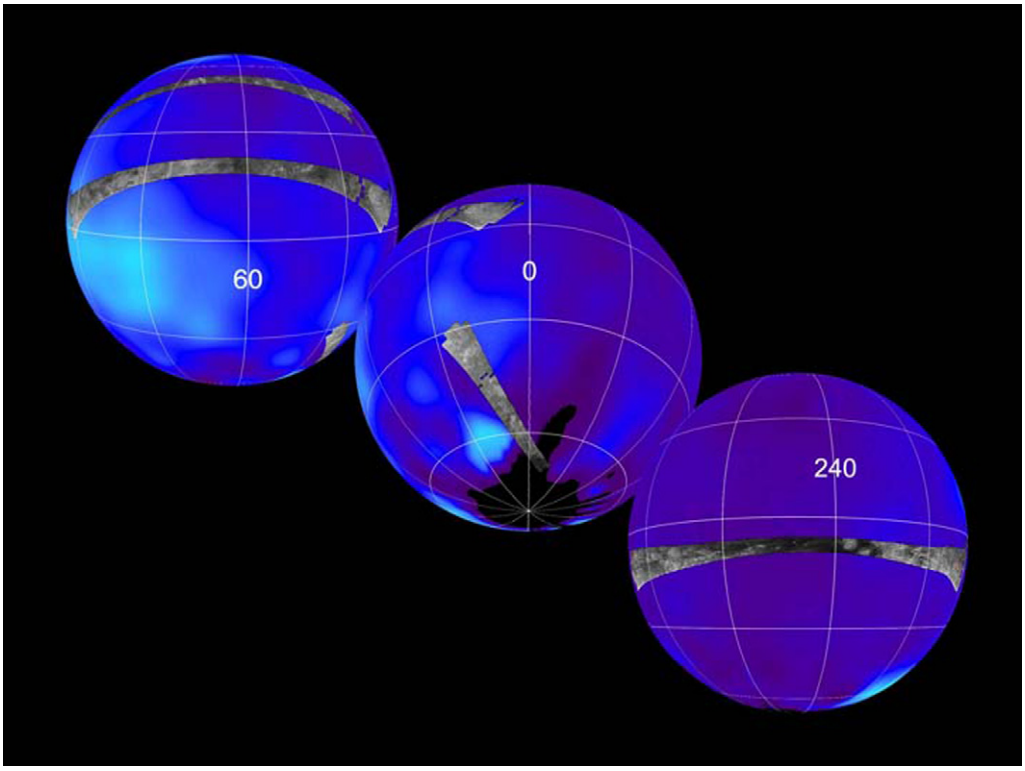

Fig. 1. Globe of Titan showing locations of Ta, T3, T7 and T8 data swaths. The swaths are superposed on globes composed of false color images from the Hubble Space Telescope. The top globe shows the Ta and T3 swaths, the middle globe shows the edge of the T3 swath and the T7 swath, and the bottom globe shows the T8 swath. See Table 1 for exact locations and dimensions of the Ta and T3 swaths.

3. Description of the radar swaths

3.1. The Ta swath

The Ta swath extends from about 130° to 10° longitude, in an arc-shaped, ∼200 km wide strip spanning latitudes from 32 to 53° N (Fig. 1). The incidence angle range across the swath varies from 2° to 46°. Six surface units were mapped in the Ta SAR swath, defined on the basis of brightness variations, general planform shape and texture (Elachi et al., 2005) (Fig. 2, Table 2). In addition, several features were mapped, including channel-like features, and irregular circular features interpreted as calderas (Elachi et al., 2005).

Two units were mapped that dominate the swath: a homogeneous unit and a mottled unit (Fig. 4). We have broadly classified these as plains units, as they are extensive, relatively featureless, and appear to be generally topographically level. The homogeneous unit (unit hu) has relatively low backscatter (Table 2) and is mostly, but not completely, featureless (Fig. 2). The homogeneous unit contains scattered bright spots and patches of variable backscatter with indistinct boundaries. The mottled unit (unit mu) has moderate to bright backscatter (Table 2) and gradational boundaries. The mottled unit occurs in patches ranging from 10's to 100's of km across.

The four other units mapped are the bright lobate unit, the dark mottled unit, the bright mottled unit, and the bright lineated unit (Elachi et al., 2005) (Fig. 4). The bright lobate unit (unit blu) occurs in several locations in the Ta swath, and has variable brightness and lobate boundaries varying from distinct to gradational. At two locations, the unit appears to emanate from circular features, which, along with its lobate boundaries, leads us to interpret this unit as cryovolcanic in origin (Elachi et al., 2005; Lopes et al., 2006). The dark mottled unit (unit dmu) forms irregularly shaped patches 10's–100's km across. In several places, they form crescent or oxbow shapes (Lorenz et al., 2005). The bright mottled unit (unit bmu) occurs in irregular, small patches in the homogeneous unit. The bright lineated unit (unit blnu) has parallel, bright lineations spaced 1–2 km apart, relatively distinct boundaries, and is found as a relatively small (<150 km across) unit in two locations.

The most conspicuous feature in the Ta swath is the large circular feature Ganesa Macula (Fig. 4f) (Elachi et al., 2005). Ganesa (∼180 km in diameter) is radar-bright at the edges, particularly at the southern edges facing the radar, consistent with the shading that would be seen on a positive relief feature with steep sides and a relatively flat top. It is somewhat similar in appearance to steep-sided domes on Venus; however, a lack of topographic information does not allow us to distinguish between a dome or shield. On the basis of its positive relief and overall radar appearance, we interpret Ganesa to be a cryovolcanic feature (Elachi et al., 2005; Lopes et al., 2006). Two units are mapped associated with Ganesa Macula: the Ganesa dark materials unit (unit gdm) and the Ganesa mottled materials unit (unit gmm). The Ganesa dark unit corresponds to the upper portions of the feature, and is cut by numerous channels, bright flows and an apparent caldera at the center of the dark unit. The Ganesa mottled unit also contains channels, which may be of either fluvial or cryovolcanic origin, some of which terminate

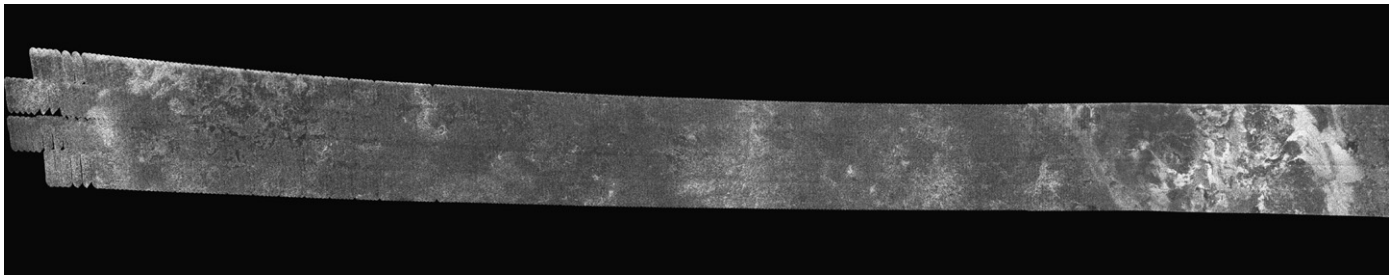

(a) Western half

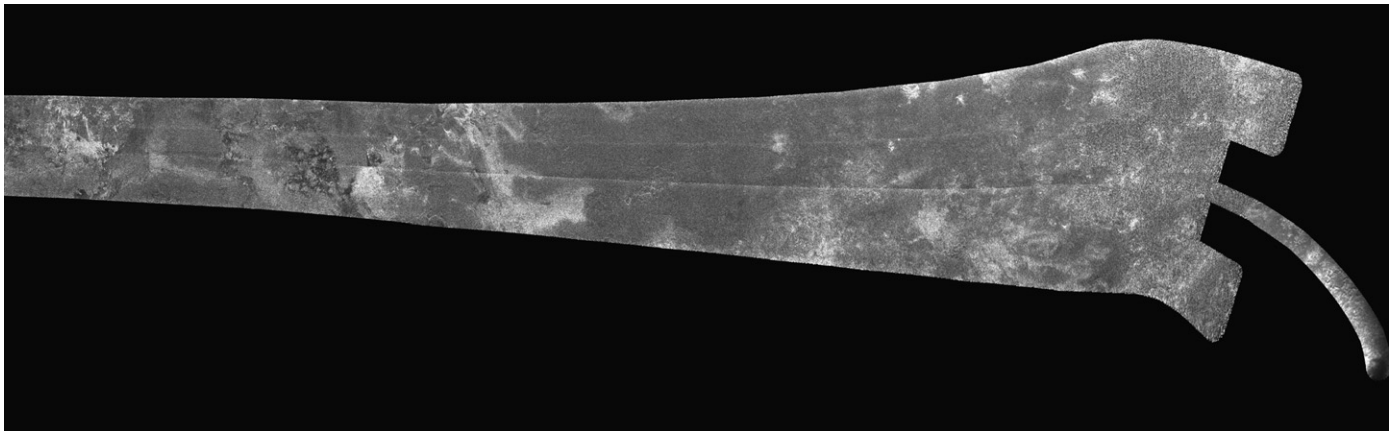

(a) Eastern half

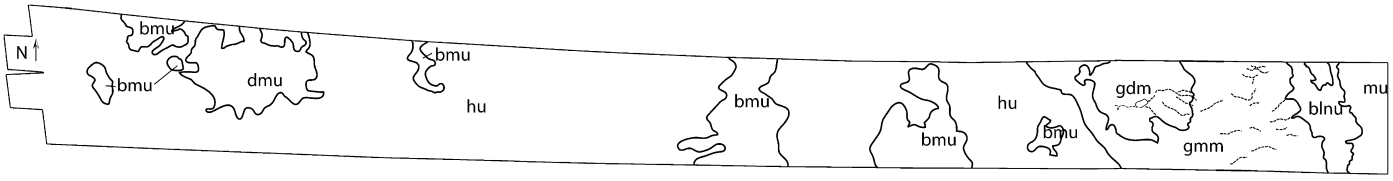

(b) Western half

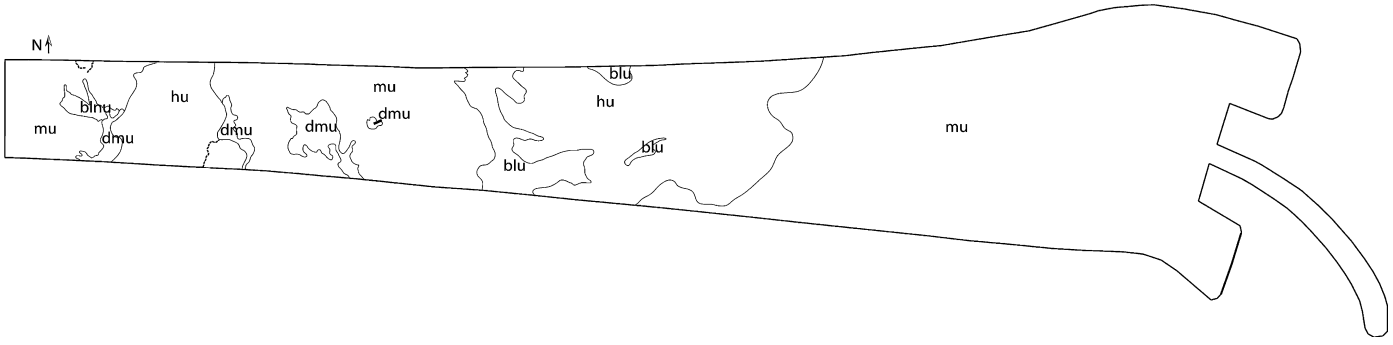

(b) Eastern half

Fig. 2. (a) Eastern and western halves of Ta data swath. Each segment is approximately 2200 km long. North is to the top of the images; the radar was left-looking, or looking from south to north. (b) Geomorphologic maps of eastern and western halves of Ta data swath. See Table 2 for unit descriptions. Each half is about 2200 km long.

in triangle-shaped features that resemble alluvial fans (Lopes et al., 2006). If the channels are fluvial then the erosive agent must be liquid methane and/or ethane, since they are the only materials stable as liquids under ambient Titan surface conditions, were detected as vapors evaporating from the surface at the Huygens landing site (Niemann et al., 2005), and are the strongest candidate erosive agents for the landing site channels (Tomasko et al., 2005).

Stratigraphically, the units associated with Ganesa Macula and the occurrences of the bright lobate unit appear to be superposed on the surrounding terrain (either the homogeneous unit or the mottled unit). We interpret both of these units to be of cryovolcanic origin, as described above (Elachi et al., 2005; Lopes et al., 2006). The easternmost patch of the bright lineated unit is embayed by the mottled unit (Fig. 4e), and thus we interpret it to be older than the mottled unit. Channels are strati-

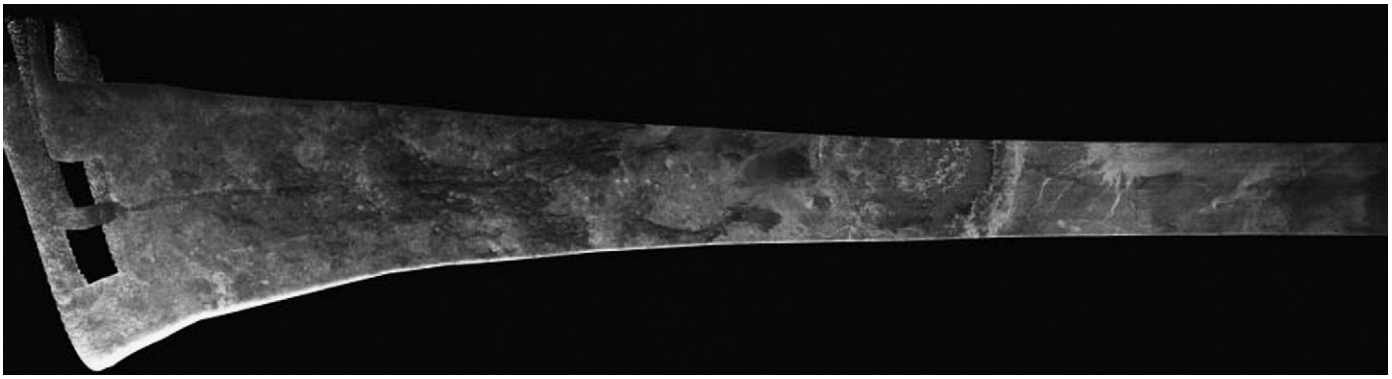

(a) Western half

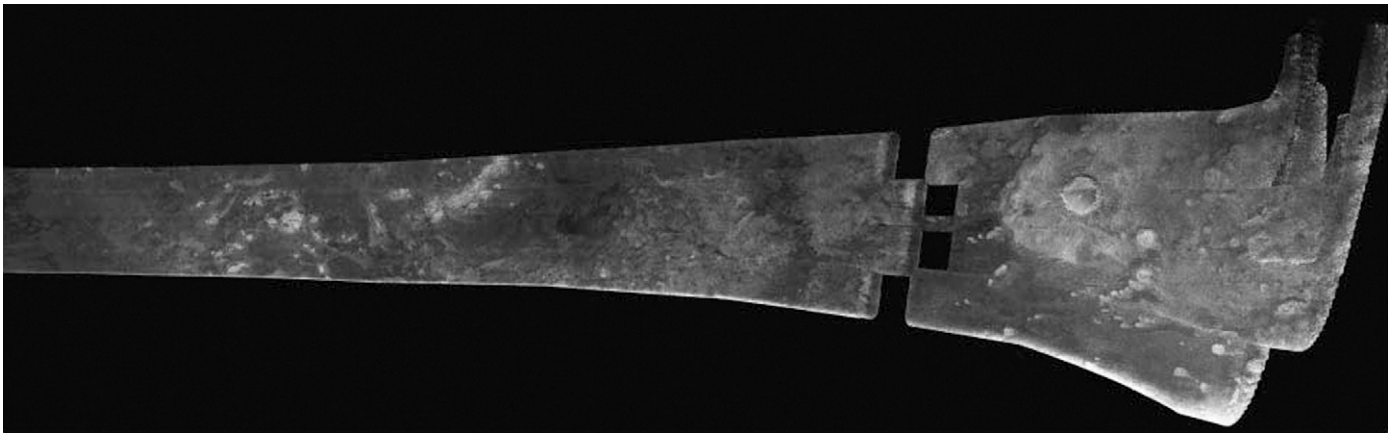

(a) Eastern half

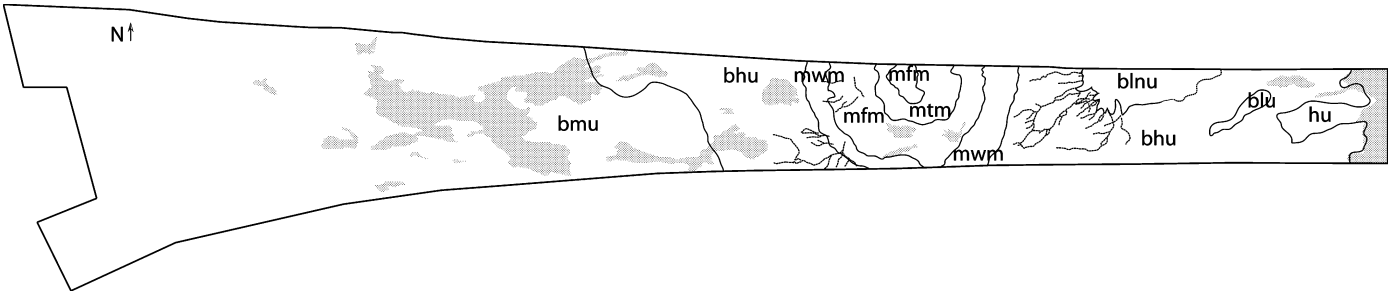

(b) Western half

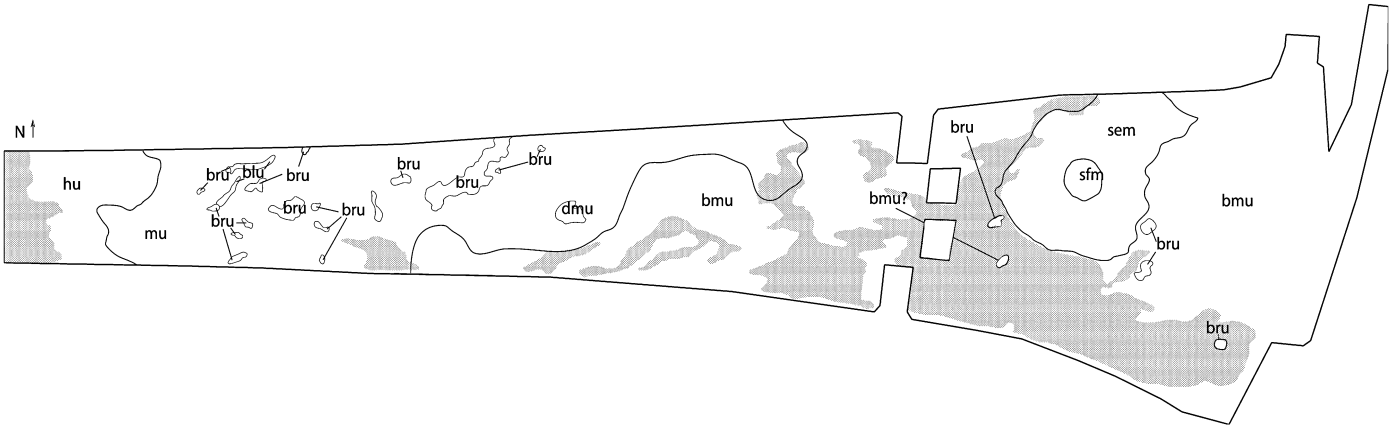

(b) Eastern half

Fig. 3. (a) Eastern and western halves of T3 data swath. Each half is approximately 3100 km long. North is to the top of the images; the radar was left-looking, or looking from south to north. (b) Geomorphologic map of eastern and western halves of T3 data swath. See Table 2 for unit descriptions. Each half is approximately 3100 km long. Shaded areas on the maps indicate location of aeolian features.

Table 2
Unit properties

Unit name	Symbol	dB range Ta*	dB range T3*	Description	Interpretation
Homogeneous unit	hu	−12.625 to −9.093	−8.687 to −7.374	Relatively featureless with low to intermediate backscatter	Plains unit composed dominantly of water ice
Mottled unit	mu	−9.883 to −7.127	−7.563 to −5.905	Variable low to intermediate backscatter at scales of 10's–100's km	Plains unit composed of fractured ice
Bright mottled unit	bmu	−8.851 to −6.617	−7.080 to −3.562	Intermediate to high backscatter unit variable at scales of 10's–100's km	Plains unit composed of rough, fractured ice
Dark mottled unit	dmu	−13.079 to −9.099		Patchy, low backscatter unit which sometimes forms crescent-shaped patches	Possible liquid hydrocarbon ponds
Bright lobate unit	blu	−7.665 to −4.234	−3.892 to −2.458	Relatively high backscatter unit with lobate boundaries	Cryovolcanic flows
Bright lineated unit	blnu	−7.230 to −3.710	−5.211 to −1.278	Relatively high backscatter unit with distinct lineations	Possible tectonically deformed materials
Ta only					
Ganesa dark materials	gdm		−11.655 to −8.506	Dark, relatively featureless unit associated with Ganesa Macula	Cryovolcanic flows
Ganesa mottled materials	gmm		−8.250 to −0.345	Intermediate to high backscatter materials associated with Ganesa Macula	Cryovolcanic flows
T3 only					
Menrva wall materials	mwm		−5.570 to −1.939	Intermediate to high backscatter unit comprising walls of Menrva crater	Impact crater wall material
Menrva textured materials	mtm		−4.618 to −2.008	Textured intermediate materials found within Menrva crater	Degraded inner ring of impact crater
Menrva floor materials	mfm		−6.839 to −3.524	Low to intermediate backscatter unit found within Menrva crater	Materials that have infilled crater floor
Sinlap floor materials	sfm		−7.053 to 3.167	Intermediate backscatter materials within Sinlap crater	Materials that have infilled crater floor
Sinlap ejecta materials	sem		−5.578 to −1.480	Intermediate to high backscatter materials surrounding Sinlap crater	Impact crater ejecta
Bright rough unit	bru		−4.780 to −0.267	High backscatter, high standing materials	Degraded hills
Bright homogeneous unit	bhu		−5.048 to −3.857	Relatively featureless unit of intermediate to high backscatter	Plains unit likely dominantly composed of fractured water ice

* The range of backscatter values (sigma0 in dB) expresses the brightness variability of the normalized radar-cross section of identified units/terrains in the swaths. The values are relative to each other within the swath; the full range of normalized data variability is +10 to −15 dB. The dB values are derived from normalized and calibrated sigma0. The calibration involves range and azimuth compression, a 2D (range, Doppler) correction, and removal of systematic variations in the amplitude due to image geometry and antenna effects (Stiles et al., 2006).

graphically young, cutting the Ganesa dark materials unit and the homogeneous unit.

3.2. The T3 swath

The T3 swath extends from 3° S to 22.5° N latitude, 0.4–133° W longitude, and is 6236 km long. Incidence angles in the swath range from 2° to 30°. The T3 swath contains five of the units mapped in the previous swath (homogeneous unit, mottled unit, dark mottled unit, bright mottled unit, and bright lobate unit), plus additional units associated with two impact craters, a bright homogeneous unit and a bright rough unit (Figs. 3 and 5; Table 2). As in the Ta swath, bright and dark channel-like features, some with associated deposits, were mapped in several locations in the swath. Additionally, about 20% of the T3 swath is characterized by parallel to sub parallel linear dark features obscure the underlying units, and are interpreted to be surficial deposits (wind streaks, dunes) on the basis of their morphology, relationship to topographic features, and superposition relationships (Lorenz et al., 2006). The linear dark features occur on all of the mapped units except the dark mottled unit, the bright rough unit and the bright lobate unit.

The most extensive unit in the T3 swath is the bright mottled unit characterized by irregular bright patches of variable size, some of which may be topographic features (Figs. 3 and 5). The bright mottled unit covers almost half of the T3 swath, but was only mapped in small patches in the Ta swath. The mottled unit is the second most extensive unit and occurs in the eastern half of the swath. The unit has moderate to bright backscatter, gradational boundaries, and contains patches of the dark mottled unit and the bright rough unit. The homogeneous unit occurs in the eastern portion of the swath, has low backscatter and is relatively featureless. The bright homogeneous unit (unit bhu) occurs in the center of the T3 swath, and contains the large impact basin, Menrva, and numerous channel-like features. Three features in the T3 swath are similar to the bright lobate unit

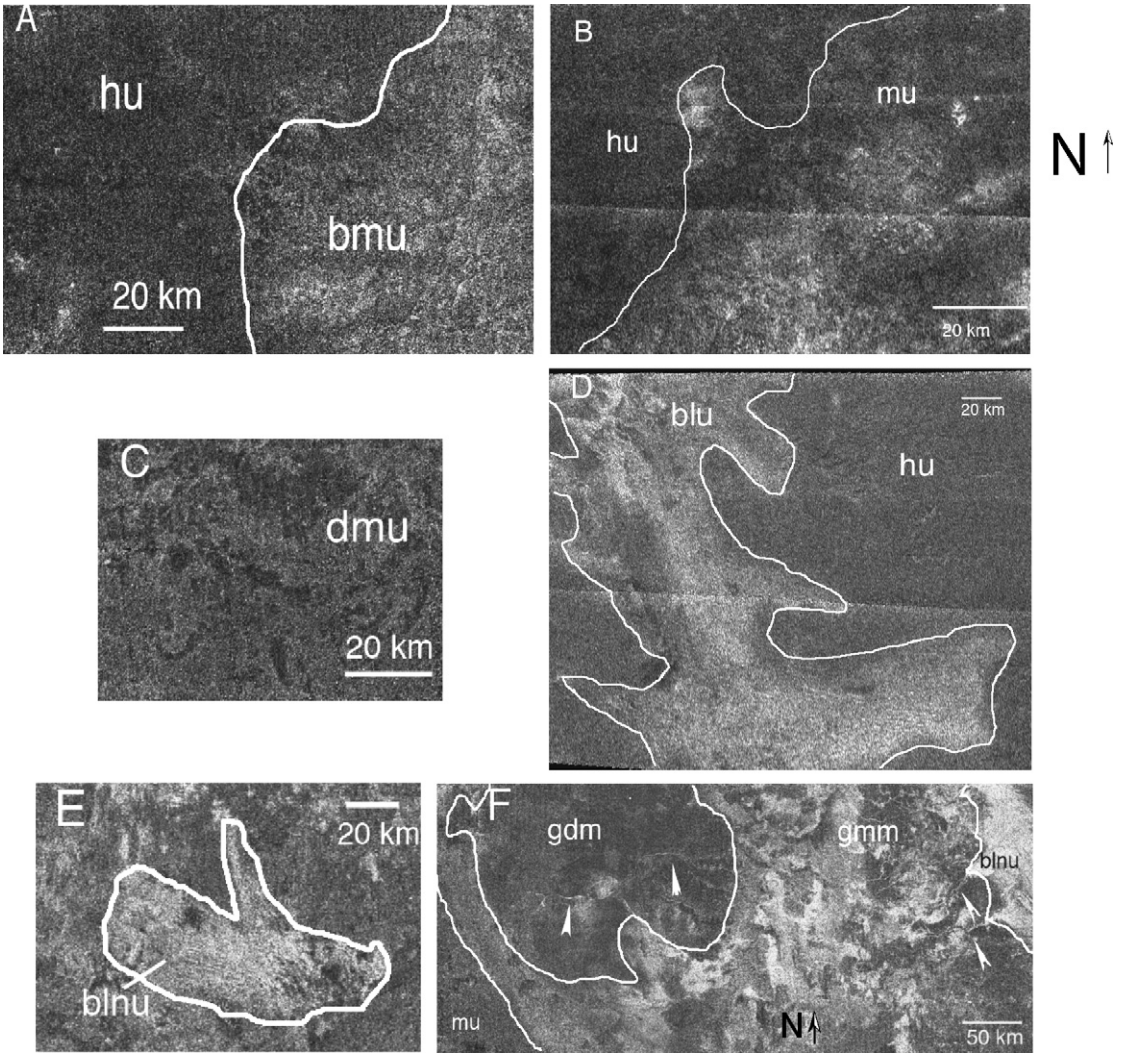

Fig. 4. SAR images of Ta units. In all of the images, north is to the top, and the radar was north-looking. (a) Homogeneous unit (hu) and bright mottled unit (bmu). Incidence angles vary from about 30°–35°. (b) Mottled unit (mu). Incidence angles vary from about 13°–24°. (c) Dark mottled unit (dmu). Incidence angles vary from about 35°–40°. (d) Bright lobate unit (blu). Incidence angles vary from about 13°–24°. (e) Bright lineated unit (blnu). Incidence angles vary from about 24°–30°. (f) Units associated with Ganesa Macula: Ganesa dark unit (gdm) and Ganesa mottled unit (gmm). Arrowheads point out channels on top of Ganesa and off its eastern flank. The alluvial-fan like features are associated with the two eastern channels. Incidence angles vary from about 24°–35°. See Table 2 for interpretations and descriptions.

identified in the Ta swath. Diffuse, somewhat lobate deposits appear in T3 in association with two bright hills and a circular feature. This unit may be cryovolcanic in origin, but the interpretation is less clear than for the Ta features, especially for the two wispy occurrences associated with the small hills of the bright rough unit (Fig. 6). The dark mottled unit occurs in several small, irregularly shaped patches (10's km across) on the mottled unit and the bright mottled unit at the eastern end of the swath. Elachi et al. (2005) interpreted the dark mottled unit in the Ta swath to be smooth deposits, consistent with possible ponds of hydrocarbons.

In the eastern portion of the T3 swath, we have mapped the bright rough unit (unit bru), which consists of high-standing 5–15 km wide features that appear to be topographically rugged based on their bright-dark pairings and surrounding, diffuse materials that are potentially erosional blankets (Radebaugh et al., 2006). In T3, the unit occurs as isolated features in the easternmost third of the T3 swath and more chain-like features in the center of the swath. Evidence for similar features in Ta is limited to a field of low (∼100 m high) hills in the easternmost and lowest resolution portion of the image (Kirk et al., 2005). Radarclinometric measurements indicate that some outcrops of the bright rough unit have slopes in excess of 10° and heights up to 500 m (Kirk et al., 2005; Radebaugh et al., 2006).

Two impact craters have been mapped in the T3 swath: Menrva (87° W, 19° N, 450 km diameter) and Sinlap (16° W, 11° N, 80 km diameter) (Fig. 3). Three units have been mapped at Menrva: a floor materials unit (unit mfm), a wall materials unit (unit mwm) and a textured materials unit (unit mtm) (Fig. 5). No clear ejecta materials can be identified at Menrva and the crater is degraded, with clear erosion of the rim (Elachi

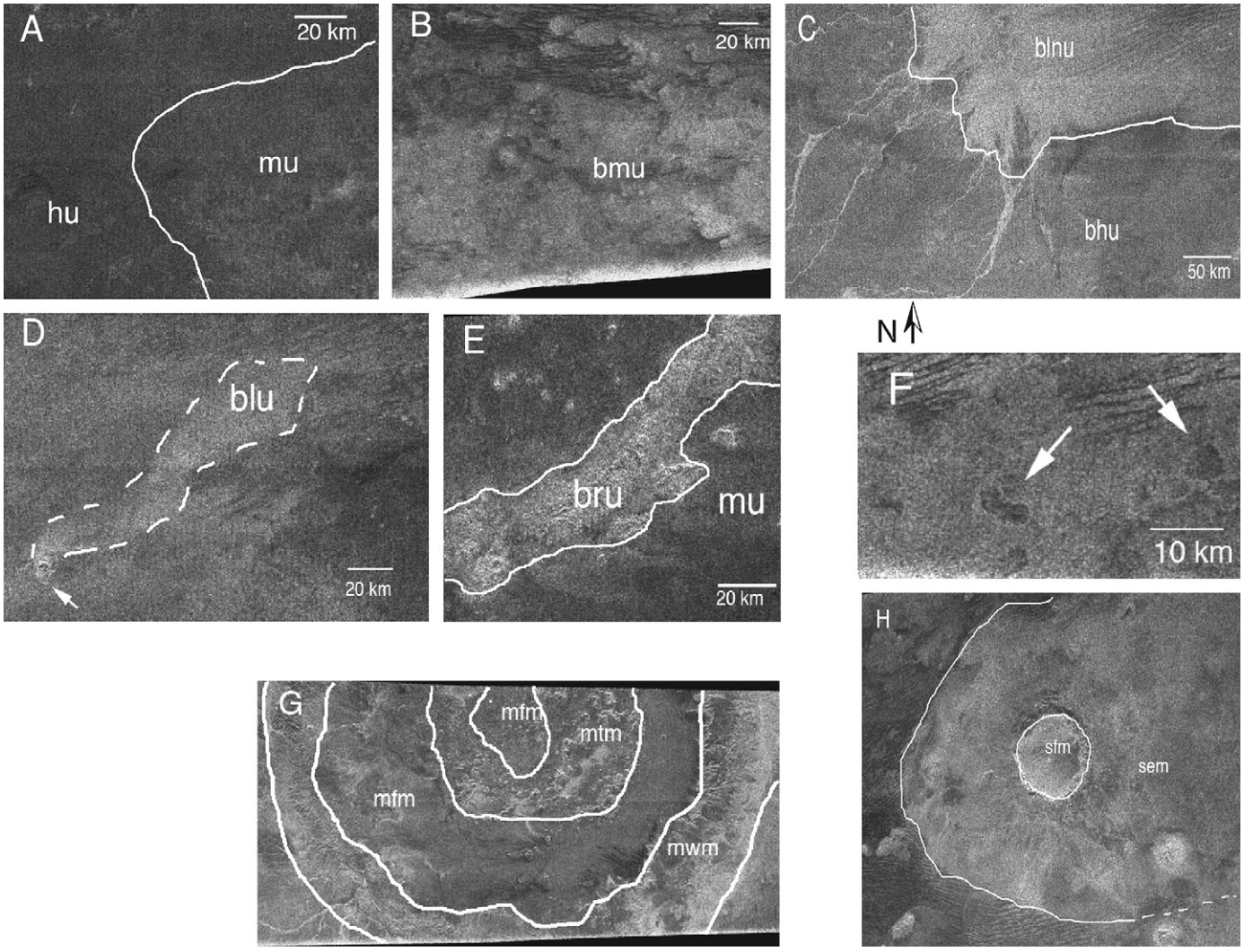

Fig. 5. Images of T3 units. In all of the images, north is to the top, and the radar was north-looking. (a) Homogeneous unit (hu) and mottled unit (mu). Incidence angles vary from about 15°–23°. (b) Bright mottled unit (bmu). Incidence angles vary from about 11°–26°. (c) Bright homogeneous unit (bhu) and bright lineated unit (blnu). Incidence angles vary from about 19°–26°. (d) Bright lobate unit (blu) associated with small circular feature (arrows). Incidence angles vary from about 19°–26°. (e) Bright rough unit (bru). Incidence angles vary from about 15°–23°. (f) Arrows point to dark mottled unit (dmu). Incidence angles vary from about 19°–26°. (g) Units associated with Menrva crater: Menrva wall materials (mwm), Menrva floor materials (mfm) and Menrva textured materials (mtm). Incidence angles vary from about 4°–23°. (h) Units associated with Sinlap crater: Sinlap ejecta materials (sem) and Sinlap floor materials (sfm). See Table 2 for interpretations and descriptions. Incidence angles vary from about 11°–23°.

et al., 2006). Dark streaks interpreted to be aeolian features are mapped within the interior of the crater. Also found in the interior and exterior of the crater are sinuous bright features. These features are interpreted to be fluvial in origin, as their morphology is consistent with formation by low viscosity fluids (such as methane or ethane), they appear to be topographically controlled, and there are no apparent cryovolcanic sources (Elachi et al., 2006). We interpret the Menrva textured materials unit to be the degraded inner ring of a double-ring basin. Two units were mapped at Sinlap: Sinlap ejecta materials (sem) and Sinlap floor materials (sfm) (Fig. 5). Sinlap is much less degraded than Menrva, and has a flat, featureless floor without a central peak. Small patches of dark material are seen in the ejecta and interior of Sinlap, suggesting some modification of the crater. However, the bulk of the floor of the crater is relatively radar-bright, indicating that smooth materials such as a deep layer of fine debris or cryolavas have not ponded extensively in the crater interior. Some dark streaks cover the crater while others bend around the crater, indicating that the ejecta at least partially serves as a topographic barrier to windblown fine materials.

Stratigraphic relations can be determined for the two impact craters and the bright rough unit, with the bright rough unit embayed by and thus older than the surrounding mottled and bright mottled units. Sinlap crater superposes the bright mottled unit, while Menrva crater is embayed by the materials of the bright homogeneous unit. The bright lobate unit superposes the mottled unit and the bright homogeneous unit. The channels in the T3 swath are stratigraphically young, cutting units bhu, mwm, and mfm.

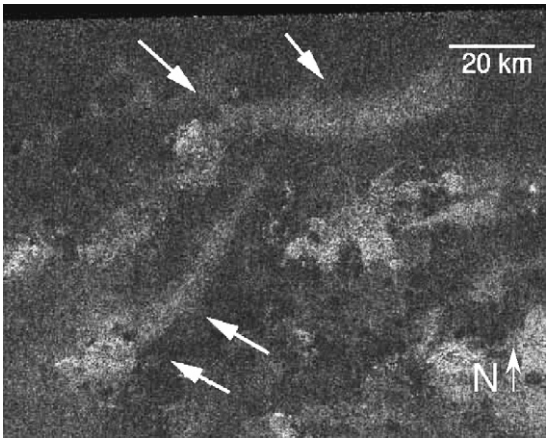

Fig. 6. Possible occurrences of bright lobate unit (blu) in the T3 swath (arrows). Both wispy, bright deposits originate at small hills, and may be either aeolian or volcanic in origin. North is to the top, and the radar was north-looking. Incidence angles vary across the image, and are typically 15°–26°.

4. Discussion

The interpretation of the units is based primarily on their appearance in the radar images, with the normalized and incidence angle corrected radar return of the images, expressed in dB, providing improved image contrast and interpretability (e.g., Stiles et al., 2006). The range of variability of the observed units (Table 2) is somewhat comparable to the backscatter return from planetary rock-strewn surfaces and Earth-like surfaces in which variations in radar backscatter are a combined effect of surface roughness, topographic variation, and dielectric properties (e.g., Campbell, 2001). However, in regard to dielectric properties, the unusual materials present on Titan's dry icy surface, such as a mix of hydrocarbons or tholins, water ice, and/or water–ammonia ice (Janssen et al., 2004; Elachi et al., 2005), reduce the dielectric variability to values in the range of 2 (hydrocarbons) to 4.5 (ammonia–water ice). This in turn could result in reduced backscattering compared to analogous surfaces of rocky materials characterized by a higher dielectric constant. Locally, volume scattering might play an important role by contributing to the high backscatter return and its variability, especially in the presence of absorbing-porous low loss tangent materials on the surface, which could account for 30% of the effective return (Janssen et al., 2004; Paganelli et al., in preparation).

4.1. Plains units

Initial altimetry results, not taken over the areas mapped by SAR to date, indicate that the small portion of Titan's surface mapped by the radar is relatively flat (Elachi et al., 2005). The units that are broadly classified as plains units are the homogeneous unit, bright homogeneous unit, the bright mottled unit, and mottled unit (Figs. 4 and 5). These units are grouped as plains units as they all cover large expanses of terrain and are likely to be relatively flat, although some may stand at higher levels than others. These units are likely to be composed dominantly of water ice, with some degree of likely contamination by tholins and hydrocarbons (McCord et al., 2006).

What is causing the variations in brightness in these units? The well-delimited, continent-like region of Xanadu that appears bright in ISS, VIMS, Keck and Hubble Space Telescope data corresponds in part to the bright mottled unit of westernmost T3, and both impact craters are seen in ISS and VIMS data. However, initial analysis indicates that other bright and dark variations seen in the radar data do not correlate well with brightness variations in other data sets. A correlation between SAR-bright and radiometric cold regions, SAR-dark and radiometric warm regions has been observed extensively in association with diverse geological features, which suggests that the correlation is not caused by a specific geologic process but characterizes the constituent material and surface properties of the features (Paganelli et al., in preparation). The observed variations in radar backscatter can be caused by surface roughness, topographic variation, and/or dielectric properties of unusual materials (mix of hydrocarbons or tholins, water ice, and more speculatively water–ammonia ice) (Janssen et al., 2004; Elachi et al., 2005, 2006). In addition, volume scattering due to subsurface structure might play a role and contribute to the high backscatter return. The correlation of SAR-bright and radiometric cold regions suggests volume scattering due to an inhomogeneous subsurface such as broken low-loss water ice or higher dielectric constant materials (Elachi et al., 2005; Ostro et al., 2006). Choosing between the latter two mechanisms is possible only if the same area is covered in dual polarization, allowing the polarization dependency of the brightness to be determined (Ostro et al., 2006). Some small radar bright spots within the plains can be attributed to possible topographic effects, but these tend to be isolated features within the plains units. Generally radar brightness caused by topographic variations will be positively correlated with radiometric brightness. It is likely that the mottling of plains units is dominated by roughness variations caused by fracturing and erosion of Titan's icy surface, with contributions from a combination of volume scattering and/or compositional variations. The plains units are unlikely to be actual geologic units, as they have gradational boundaries and unclear stratigraphic relationships. Their relatively bland surface character provides little insight into their mode of origin; further studies combining radar, ISS and VIMS data may provide insight into the origin of these expansive units on Titan.

The most remarkable thing about the plains units is the lack of impact craters. Prior to Cassini, it had been assumed that if the surface of Titan were not obscured by widespread, deep, hydrocarbon oceans, the surface of Titan would have a relatively high population of impact craters (Lorenz, 1997), although scenarios for a more active Titan had been proposed (e.g., Stevenson, 1992).

5. Evidence for endogenic processes

Much of the interior of Titan may have melted during accretion, owing to its size, and thus the interior of Titan may have a significant layer of water–ammonia liquid (Lunine and

Stevenson, 1987; Tobie et al., 2005; Mitri et al., 2006). During the orbital evolution of Titan, variations in the interior heat flux may have produced repeated changes from a convective to a conductive configuration of the ice shell, causing large variations in thickness over relatively short time scales. This regime could cause fracturing of the surface as well as allow for cryovolcanism (Mitri and Showman, 2005; Mitri et al., 2006). Some of these events could have occurred relatively recently (i.e., within the last 500 myr) (Tobie et al., 2006). Evidence for endogenic processes on Titan is provided by the bright lobate unit, Ganesa Macula, and possibly by the bright lineated unit and bright rough unit.

5.1. Bright lobate unit and Ganesa Macula

The bright lobate unit and Ganesa Macula provide strong evidence that cryovolcanism has occurred on Titan (Elachi et al., 2005; Lopes et al., 2006). In the two occurrences in the Ta swath and the three occurrences in the T3 swath, the bright lobate unit appears to extend from a circular depression or small hill. We interpret the circular depressions in the Ta swath to be calderas. In another location in the Ta swath, a long (>200 km) lobate flow complex extends across the swath, emanating from an unknown source to the northwest of the swath (Fig. 4d). This flow has an area of at least 23,700 km^2, and strongly resembles lobate flow units seen in radar data of Venus and Earth (Lopes et al., 2006). The occurrences of the bright lobate unit in the T3 swath have less distinct boundaries, and therefore are somewhat less reliably interpreted as cryovolcanic in origin.

As described above, we interpret Ganesa Macula as a cryovolcanic construct, either a dome or a shield, and we interpret several other features, including circular features with associated flows, as cryovolcanic in origin (Lopes et al., 2006). Their resemblance to features that on Earth are associated with basaltic volcanism suggest mobilization of crustal material with a mobility akin to that of basalt (Lopes et al., 2006). If the crust of Titan is largely water ice, as suggested by interior models (Lunine and Stevenson, 1987) and spectroscopic data (Lellouch et al., 2004), then flows of water mixed with ammonia or ammonia and methanol provide higher viscosities (Kargel et al., 1991), although the presence of crystals within the melt may be required to obtain a mobility equivalent to basalt (Mitchell et al., 2006). One other possible volcanic edifice at 8.5°, −143.5° on Titan has been identified in VIMS data (Sotin et al., 2005), but has not been imaged by the radar. Some small circular features in the T8 swath have been tentatively interpreted as cryovolcanic in origin, while no cryovolcanic features were identified in the T7 swath. Too little of Titan has been imaged to date to conjecture on the global distribution of cryovolcanic features. Theoretical estimates of resurfacing by cryovolcanism are equivalent to a global layer up to several kilometers in thickness, enough to bury most topographic features including large but viscously relaxed craters (see below) (Lopes et al., 2006).

5.2. Tectonism on Titan?

Little evidence for tectonic activity is seen in these first two radar swaths. No extensive bright lineaments suggestive of faults or fractures are seen cutting any of the plains units. The bright lineated unit in the Ta swath occurs in two patches, one associated with channels and Ganesa Macula, and the other in a small angular patch. The bright lineated unit in the T3 swath is also associated with channels. Both of these channel-associated bright lineated units are less likely to be tectonic in origin, than to have been produced by flow or by overlying streaks of dark material similar to the T3 dark lineations, which are likely to be aeolian in origin. We interpret the angular patch of bright lineated material in the Ta swath (Fig. 4e) to be more likely tectonic in origin, due to its more distinct bright and dark lineations and angular boundaries. This may be a patch of lineated terrain similar to that seen on other icy satellites, which has subsequently been embayed by the mottled and dark mottled units.

The bright rough unit in the T3 swath could be remnants of tectonically produced ridges, cryovolcanic features or impact crater rims. The impact origin is slightly less likely, as the hills are not arranged in any clear circular pattern. The small number of outcrops of this unit and their irregular distribution prevent a reliable interpretation at this time.

6. Exogenic processes

Exogenic processes are also playing a role in resurfacing Titan. Data from the Huygens probe have demonstrated that liquids from rainfall or sapping have flowed across the surface (Tomasko et al., 2005), and channels have been identified in all of the four radar swaths collected to date (Elachi et al., 2005, 2006; Lorenz et al., in preparation; Lunine et al., in preparation). In addition, the T3 swath has illustrated the potential importance of aeolian process on Titan.

6.1. Channels

Channels (0.5–1 km wide, 10's km long in Ta and up to 200 km long in T3) are mapped in both swaths, commonly in association with fan-shaped deposits. Some of the channels may be cryovolcanic in origin, particularly those associated with Ganesa Macula. Huygens probe data revealed the presence of many small-scale (10–30 m wide, few km long) channels that are interpreted to be consistent with rainfall, others that appear to have run along a fracture system, and the probe landing site is dominated by rounded stones likely shaped by transport in a stream or river (Tomasko et al., 2005). Some of these channel networks appear characteristic of pluvial processes, while others suggest a sapping origin. The bulk of the channels we have observed in T3 are likely to have been cut by liquid methane (or ethane, since its physical properties are similar and is fully miscible with methane) in one or more violent pluvial events (Lorenz et al., in preparation). We note that all the T3 fluvial channels appear to be close to Menrva, although this may be purely coincidental. A large number of channels have also been identified in the T7 swath, though few are seen in the T8

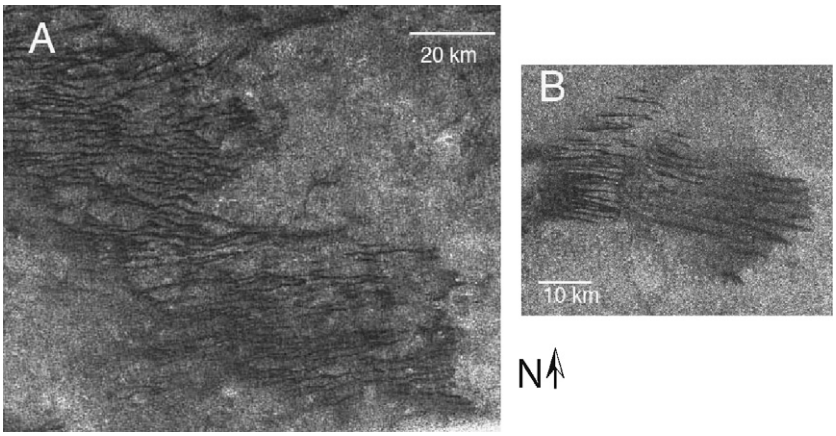

Fig. 7. (a) An example of dune-like features from the T3 swath. Note the abrupt western terminations that may indicate a topographic boundary. Incidence angles across the image vary from about 15°–26°. (b) Streaks from the T3 swath. In both of the images, north is to the top and the radar was north-looking. Incidence angles vary across the images, and are about 15°–23°.

swath. As with cryovolcanic features, the distribution and frequency of likely features produced by flowing liquids are still unknown, and unfortunately, the two-order-of-magnitude difference in width between the Huygens DISR channels and those detectable by radar inhibit an understanding of the relationship between the two.

6.2. *Ponds?*

The dark mottled unit in the Ta swath contains many oxbow and irregular dark patches that could be ponds or lakes of liquid hydrocarbons (Lorenz et al., 2005; Elachi et al., 2005). The dark mottled unit in the T3 swath is a smaller occurrence than the patches in the Ta swath, and does not contain the distinct, very-dark, possible ponds. The lack of specular reflection seen in imaging data of Titan argue against large expanses of exposed liquid hydrocarbons (West et al., 2005), but does not militate against the radar-dark patches being filled with liquid. Recent theoretical studies with a global circulation model (GCM) by Rannou et al. (2006) suggest that low latitudes on Titan should become desiccated with time unless methane is resupplied volcanically, while high latitudes may be saturated. While this does not confirm that the dark ponds in TA are liquid, their prevalence in TA compared with the lower-latitude T3 is consistent with the latitudinal trend suggested in the GCM.

6.3. *Aeolian features*

The dark, generally linear, streak-like features that cover parts of the T3 swath are interpreted to be aeolian in origin based on their morphology and similarity to aeolian features on Earth (Elachi et al., 2006; Lorenz et al., 2006), although the features observed in T3 do not appear to have substantial relief, compared to the ∼100 m height of similar features observed closer to the equator on T8 (Elachi et al., 2006; Lorenz et al., 2006). Some of the dark linear features are quite long, uniform in width, and have 'tuning fork' junctions; these features are interpreted to be longitudinal dunes (Fig. 7a) (Lorenz et al., 2006). Others are more irregular in width and are associated with dark patches, and may be wind streaks (Fig. 7b). The dark linear features in the T3 swath are superposed on the other units, and form irregularly shaped patches as large as 400 km across. It is possible that the dark linear features are forming in topographic lows; some patches appear to terminate abruptly suggesting topographic boundaries (Fig. 7a).

The presence of aeolian features on Titan is consistent with its low gravity and dense atmosphere, and models and observations of wind speeds (Lorenz et al., 1995, 2006). The presence of dunes and streaks also indicates a significant supply of particulate material, in the size range of 0.18–0.25 mm (Lorenz et al., 2006). Processes that can produce particulate material (in this case, ice particles and possibly tholins) include impact cratering, explosive volcanism, deposition of material from the atmosphere, and erosion by fluvial and/or aeolian processes. No evidence of explosive cryovolcanism has been found to date (Lopes et al., 2006), and the paucity of impact craters suggests that any impact-produced regolith has been subsequently buried or reworked. Erosion by wind and liquid hydrocarbons along with atmospheric deposition are the most likely processes producing the bulk of the particulate material. The Huygens landing site seemed to be characterized by a surface that might contain liquids (Zarnecki et al., 2005); some examples of dry or non-sticky materials must be present on Titan in order to produce particulate matter for the dunes. The radar-bright substrate beneath the linear features, their moderately limited extent, and their apparently low relief, may suggest that the supply of sand-sized material is limited in the regions imaged in T3.

6.4. *Impact cratering*

Two impact craters, Menrva and Sinlap, have been identified in the T3 swath; no undisputed impact craters are seen in any other of the Titan swaths. Small (∼5 km) indistinct circular features of unknown origin are seen in both the Ta and T3 swaths (Fig. 8). These could be highly eroded impact craters or cryovolcanic calderas or pits. These features are below the formal end of the size range for impact craters that could be formed on Titan owing to its thick atmosphere (Lorenz, 1997). In addition,

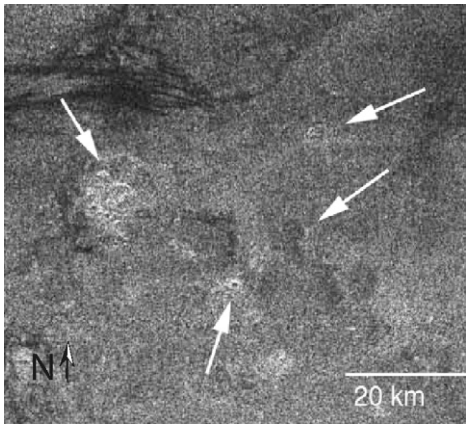

Fig. 8. Arrows indicate small circular features (<8 km diameter) from the T3 swath. The features may be impact or cryovolcanic in origin. North is to the top, and the radar was north-looking. Incidence angles vary across the image, and are approximately 23°–30°.

their relatively confined size range (there are no intermediate-sized impact craters as noted below) and their similarities to depressions associated with flows in the Ta swath lead us to tentatively favor a cryovolcanic origin for these features.

Menrva crater appears to be relatively old, as it has been modified by aeolian and fluvial processes. Sinlap crater is less degraded, and probably formed more recently. The scarcity of craters in the 20–100 km size range indicates that the sections of Titan imaged by the radar to date are relatively young (Elachi et al., 2006). The 450 km diameter Menrva basin may provide evidence for the preservation of some very old (∼few Gyr) surfaces on Titan, but its peculiar shape also suggests that the crater was flooded during formation, consistent with a liquid layer below a roughly 50 km diameter crust (Lunine et al., 2005). The absence of a central peak in the smaller crater Sinlap is mysterious, and suggests two possibilities. One is that the crater formed when the crust of Titan was thinner than at the time and/or place that Menrva formed, suggesting significant spatial or temporal variations in crustal thickness (Tobie et al., 2006). Alternatively, the central peak of Sinlap may be buried by photochemical or volcanic materials that have filled the crater. This would require the crater to be significantly relaxed in order for the peak to be plausibly buried (even if it were partially eroded). Such topographic relaxation is expected on Titan because of the relatively thin, rigid lithosphere over its history (Lunine et al., 2005; Tobie et al., 2006), but detailed modeling of this specific crater is strongly warranted given the lack of a central peak. A second radar pass over either or both craters, with a trajectory oblique to the first, would be of extreme scientific value in allowing the topography of these craters to be constrained, thus helping to constrain the crustal thickness and geological processes of erosion and burial.

7. Conclusions

The Ta and T3 swaths differ dramatically from each other, making it difficult at present to assess the overall balance of processes at work on Titan's surface (Lorenz and Lunine, 2005). The Ta swath is dominated by processes such as cryovolcanism, possible occurrence of fluvial channels and lakes, and some tectonic activity. While T3 includes large areas with dunes, they are interrupted by the poorly understood mottled unit, and T3 contains two very large and very different impact craters. The overall paucity of impact craters indicates that the surface we have imaged to date is relatively young, with evidence for resurfacing by cryovolcanism, fluvial erosion, and aeolian erosion. Atmospheric deposition of materials is also likely to contribute to resurfacing. With the little radar data we have received to date, there is some evidence of trends with latitude, with aeolian features dominant in the equatorial dark regions and perhaps more evidence of liquids at higher latitudes. The question of 'What is Titan like?' clearly has no simple answer; even the limited amount of data in hand indicate that the surface of Titan could be comparable in variety to that of Earth.

The very different geologic surfaces revealed by the swaths may in part be an artifact of the scant coverage achieved to date with the radar, but nonetheless this hints at a complex history of this world. Titan's large size, significant rock mass fraction and modest tidal heating imply enough internal energy to maintain liquid water mixed with antifreeze in its interior (Tobie et al., 2005), but the extent to which outgassing or cryovolcanism have occurred remain difficult to predict because of the potential difficulty of moving liquid water through a thick ice crust (even with ammonia lowering the density). Further Cassini Radar, and other remote sensing data, will therefore be crucial in testing our idea that relatively youthful cryovolcanic features are present on the surface, and in identifying tectonic features that will provide some insight into processes of crustal deformation and potential mechanisms of resurfacing. The limited amount of radar coverage expected by the end of the prime mission, up to 20%, will unfortunately limit our ability to interpret Titan in terms of the global balance of endo- and exogenic processes, and hence extended mission radar coverage is essential if we are to understand the nature of and extent to which internal and external processes have shaped Titan's surface.

Acknowledgments

We gratefully acknowledge the long years of work by the entire Cassini team that allowed these data of Titan to be obtained. The Cassini Project is a joint endeavor of NASA, ESA and ASI, and is managed by the Jet Propulsion Laboratory, California Institute of Technology under a contract with NASA. Helpful reviews by George McGill and Rebecca Ghent improved this manuscript.

References

Bender, K.C., Senske, D.A., Greeley, R., 2000. Geologic map of the Carson Quadrangle (V43), Venus. U.S. Geological Survey Geological Investigations Series Map I-2620. Scale 1:5,000,000.

Campbell, B., 2001. Radar backscatter from Mars: Properties of rock-strewn surfaces. Icarus 150, 38–47.

Elachi, C., 1987. Introduction to the Physics and Techniques of Remote Sensing. John Wiley and Sons, New York. 413 pp.

Elachi, C., Im, E., Roth, L.E., Werner, C.L., 1991. Cassini Titan Radar Mapper. Proc. IEEE 79, 867–880.

Elachi, C., Wall, S., Allison, M., Anderson, Y., Boehmer, R., Callahan, P., Encrenez, P., Flamini, E., Franceschetti, G., Gim, Y., Hamilton, G., Hensley, S., Janssen, M., Johnson, W., Kelleher, K., Kirk, R., Lopes, R., Lorenz, R., Lunine, J., Muhleman, D., Ostro, S., Paganelli, F., Picardi, G., Posa, F., Roth, L., Seu, R., Shaffer, S., Soderblom, L., Stiles, B., Stofan, E., Vetrella, S., West, R., Wood, C., Wye, L., Zebker, H., 2005. Cassini Radar views the surface of Titan. Science 308, 970–974.

Elachi, C., Wall, S., Janssen, M., Stofan, E., Lopes, R., Kirk, R., Lorenz, R., Lunine, J., Paganelli, F., Soderblom, L., Wood, C., Wye, L., Zebker, H., Anderson, Y., Ostro, S., Allison, M., Boehmer, R., Callahan, P., Encrenaz, P., Flamini, E., Francescetti, G., Gim, Y., Hamilton, G., Hensley, S., Johnson, W., Kelleher, K., Muhleman, D., Picardi, G., Posa, F., Roth, L., Seu, R., Shaffer, S., Stiles, B., Vetrella, S., West, R., 2006. Titan Radar Mapper observations from Cassini's T_A and T_3 flybys. Nature 441, 709–713, doi:10.1038/nature04786.

Ford, J.P., Plaut, J.J., Weitz, C.M., Farr, T.G., Senske, D.A., Stofan, E.R., Michaels, G., Parker, T.J. (Eds.), 1993. Guide to Magellan Image Interpretation. JPL Publ. 93-24, 148 pp.

Hansen, V.L., 2000. Geologic mapping of tectonic planets. Earth Planet. Sci. Lett. 176, 527–542.

Janssen, M.A., Lorenz, R., Elachi, C., Anderson, Y.Z., Boehmer, R.A., Gim, Y., Johnson, W.T.K., Kelleher, K.D., Kirk, R., Lopes, R.M., Paganelli, F., Roth, L.E., Wall, S.D., West, R.W., 2004. First mapping of Titan with the Cassini RADAR radiometer. DPS 36 (4). Abstract 1075.

Kargel, J.S., Croft, S.K., Lunine, J.I., Lewis, J.S., 1991. Rheological properties of ammonia–water liquids and crystal–liquid slurries: Planetological applications. Icarus 89, 93–112.

Kirk, R.L., Callahan, P., Seu, R., Lorenz, R.D., Paganelli, F., Lopes, R., Elachi, C., and the Cassini RADAR Team, 2005. Radar reveals Titan topography. Lunar Planet. Sci. XXXVI. Abstract 2227.

Lellouch, E., Schmitt, B., Coustenis, A., Cuby, J.-G., 2004. Titan's 5-micron lightcurve. Icarus 168, 209–214.

Lopes, R., Mitchell, K.L., Stofan, E.R., Lunine, J.I., Lorenz, R., Paganelli, F., Kirk, R.L., Wood, C.A., Wall, S.D., Robshaw, L.E., Fortes, A.D., Neish, C.D., Radebaugh, J., Reffet, E., Ostro, S.J., Elachi, C., Allison, M.D., Anderson, Y., Boehmer, R., Boubin, G., Callahan, P., Encrenaz, P., Flamini, E., Francescetti, G., Gim, Y., Hamilton, G., Hensley, S., Janssen, M.A., Johnson, W.T., Kelleher, K., Muhleman, D.O., Ori, G., Orosei, R., Picardi, G., Posa, F., Roth, L.E., Seu, R., Shaffer, S., Soderblom, L.A., Stiles, B., Vetrella, S., West, R.D., Wye, L., Zebker, H.A., 2006. Cryovolcanic features on Titan's surface as revealed by the Cassini Titan Radar Mapper. Icarus. In press.

Lorenz, R.D., 1996. Pillow lava on Titan: Expectations and constraints on cryovolcanic processes. Planet. Space Sci. 44, 1021–1028.

Lorenz, R.D., 1997. Impacts and cratering on Titan—A pre-Cassini view. Planet. Space Sci. 45, 1009–1019.

Lorenz, R.D., Mitton, J., 2002. Lifting Titan's Veil. Cambridge Univ. Press, Cambridge, UK.

Lorenz, R.D., Lunine, J.I., 2005. Titan's surface before Cassini. Planet. Space Sci. 53, 557–576.

Lorenz, R.D., Lunine, J.I., Grier, J.A., Fisher, M.A., 1995. Prediction of aeolian features on planets: Application to Titan paleoclimatology. J. Geophys. Res. 88, 26377–26386.

Lorenz, R.D., Elachi, C., Stiles, B., West, R.A., Janssen, M.A., Lopes, R.M., Stofan, E.R., Paganelli, F., Wood, C.A., Kirk, R.L., Lunine, J.I., Wall, S.D., 2005. Titan's elusive lakes? Properties and context of dark spots in Cassini TA radar data. Lunar Planet. Sci. XXXVI. Abstract 1682.

Lorenz, R.D., Wall, S., Radebaugh, J., Boubin, G., Reffet, E., Janssen, M., Stofan, E., Lopes, R., Kirk, R., Elachi, C., Lunine, J., Paganelli, F., Soderblom, L., Wood, C., Wye, L., Zebker, H., Anderson, Y., Ostro, S., Allison, M., Boehmer, R., Callahan, P., Encrenaz, P., Ori, G.G., Francescetti, G., Gim, Y., Hamilton, G., Hensley, S., Johnson, W., Kelleher, K., Mitchell, K., Muhleman, D., Picardi, G., Posa, F., Roth, L., Seu, R., Shaffer, S., Stiles, B., Vetrella, S., Flamini, E., West, R., 2006. The sand seas of Titan: Cassini RADAR observations of longitudinal dunes. Science 312, 724–727.

Lunine, J.I., Stevenson, D.J., 1987. Clathrate and ammonia hydrates at high pressure: Application to the origin of methane on Titan. Icarus 70, 61–77.

Lunine, J.I., Stevenson, D.J., Yung, Y.L., 1983. Ethane ocean on Titan. Science 222, 1229–1230.

Lunine, J.I., Artemieva, N., Lorenz, R., Flamini, E., 2005. Numerical modeling of impact cratering on Titan with implications for the age of Titan's surface. Lunar Planet. Sci. XXXVI. Abstract 1504.

McCord, T.B., Hansen, G.B., Buratti, B.J., Clark, R.N., Cruikshank, D.P., D'Aversa, E., Griffith, C.A., Baines, E.K.H., Brown, R.H., Dalle Ore, C.M., Filacchione, G., Formisano, V., Hibbitts, C.A., Jaumann, R., Lunine, J.I., Nelson, R.M., Sotin, C., and the Cassini CIMS Team, 2006. Composition of Titan's surface from Cassini VIMS. Planet. Space Sci. Submitted for publication.

McGill, G.E., 2000. Geologic map of the Sappho Patera Quadrangle (V20), Venus. U.S. Geological Survey Geological Investigations Series Map I-2637. Scale 1:5,000,000.

Mitchell, K.L., Lopes, R.M.C., Robshaw, L.E., Kargel, J.S., Lunine, J., Lorenz, R., Petford, N., Wilson, L., and the Cassini RADAR Team, 2006. Ascent and eruption of cryomagmas on Titan 2: Eruption styles and landforms. Lunar Planet. Sci. XXXVII. Abstract 2355.

Mitri, G., Showman, A.P., 2005. Convective conductive transitions and sensitivity of a convecting ice shell to perturbations in heat flux and tidal-heating rate: Implications for Europa. Icarus 177, 447–460.

Mitri, G., Showman, A.P., Lunine, J.I., Lopes, R., 2006. Resurfacing of Titan by ammonia–water cryomagma. Lunar Planet. Sci. XXXVII. Abstract 1994.

Muhleman, D.O., Grossman, A.W., Butler, B.J., Slade, M.A., 1990. Radar reflectivity of Titan. Science 248, 975–980.

Niemann, H.B., Atreya, S.K., Bauer, S.J., Carignan, G.R., Demick, J.E., Frost, R.L., Gautier, D., Haberman, J.A., Harpold, D.N., Hunten, D.M., Israel, G., Lunine, J.I., Kasprzak, W.T., Owen, T.C., Paulkovich, M., Raulin, F., Raaen, E., Way, S.H., 2005. The composition of Titan's atmosphere from the GCMS on the Huygens probe, and implications for the origin of nitrogen and methane. Nature 438, 779–784.

Ostro, S.J., West, R.D., Janssen, M.A., Lorenz, R.D., Zebker, H.A., Black, G.J., Lunine, J.I., Wye, L.C., Lopes, R.L., Wall, S.D., Elachi, C., Roth, L., Hensley, S., Kelleher, K., Hamilton, G.A., Gim, Y., Anderson, Y.Z., Boehmer, R.A., Johnson, W.T.K., and the Cassini RADAR Team, 2006. Cassini RADAR observations of Enceladus, Tethys, Dione, Rhea, Iapetus, Hyperion, and Phoebe. Icarus 183 (2), 479–490.

Radebaugh, J., Kirk, R., Lorenz, R., Lunine, J., and the Cassini RADAR Team, 2006. Mountains on Titan observed by Cassini Radar. Lunar Planet. Sci. XXXVII. Abstract 1007.

Rannou, P., Montmessin, F., Hourdin, F., Lebonnois, S., 2006. The latitudinal distribution of clouds on Titan. Science 311, 201–205.

Sotin, C., Jaumann, R., Buratti, B.J., Brown, R.H., Clark, R.N., Soderblom, L.A., Baines, K.H., Belluci, G., Bibring, J.-P., Capaccione, F., Cerroni, P., Combes, M., Coradini, A., Cruikshank, D.P., Drossart, P., Formisano, V., Langevin, Y., Matson, D.L., McCord, T.B., Nelson, R.M., Nicholson, P.D., Sicardy, B., LeMouelic, S., Rodriguez, S., Stephan, K., Scholz, C.K., 2005. Release of volatiles from a possible cryovolcano from near-infrared imaging of Titan. Nature 435, 786–789.

Stevenson, D.J., 1992. Interior of Titan. ESA SP-338, 167–176.

Stiles, B.W., Gim, Y., Hamilton, G., Hensley, S., Johnson, W.T.K., Shimada, J., West, R.D., Callahan, P., 2006. Ground processing of Cassini RADAR imagery of Titan. IEEE Trans. In press.

Stofan, E.R., Head, J.W., Campbell, D.B., Zisk, S.H., Bogomolov, A.F., Rzhiga, O.N., Basilevsky, A.T., Armand, N., 1989. Geology of a Venus rift zone: Beta Regio and Devana Chasma. Geol. Soc. Am. Bull. 101, 143–156.

Tobie, G., Grasset, O., Lunine, J.I., Mocquet, J., Sotin, C., 2005. Titan's orbit provides evidence for a subsurface ammonia–water ocean. Icarus 175, 496–502.

Tobie, G., Lunine, J.I., Sotin, C., 2006. Episodic outgassing as the origin of atmospheric methane on Saturn's moon Titan. Nature 440, 61–64.

Tomasko, M., Archinal, B., Becker, T., Bézard, B., Bushroe, M., Combes, M., Cook, D., Coustenis, A., de Bergh, C., Dafoe, L., Doose, L., Douté, S., Eibl, A., Engel, S., Gliem, F., Grieger, B., Holso, K., Howington-Kraus, E., Karkoschka, E., Keller, H., Kirk, R., Kramm, R., Küppers, M., Lanagan, P., Lellouch, E., Lemmon, M., Lunine, J., McFarlane, E., Moores, J., Prout, M., Rizk, B., Rosiek, M., Rueffer, P., Schröder, S., Schmitt, B., See, C., Smith, P., Soderblom, L., Thomas, N., West, R., 2005. Rain, winds, and haze during the Huygens probe descent to Titan's surface. Nature 438, 765–778.

West, R.A., Brown, M.E., Salinas, S.V., Bouchez, A.H., Roe, H.G., 2005. No oceans on Titan from the absence of a near-infrared specular reflection. Nature 436, 670–672.

Wilhelms, D.E., 1972. Geologic mapping of the second planet. U.S. Geological Survey Interagency Report. Astrogeology 55.

Wilhelms, D.E., 1990. Geologic mapping. In: Greeley, R., Batson, R.M. (Eds.), Planetary Mapping. Cambridge Univ. Press, Cambridge, UK. 296 pp.

Zarnecki, J.C., Leese, M.R., Hathi, B., Ball, A.J., Hagermann, A., Towner, M.C., Lorenz, R.D., McDonnell, J.A.M., Green, S.F., Patel, M.R., Ringrose, T.J., Rosenberg, P.D., Atkinson, K.R., Paton, M.D., Banaszkiewicz, M., Clark, B.C., Ferri, F., Fulchignoni, M., Ghafoor, N.A.L., Kargl, G., Svedhem, H., Delderfield, J., Grande, M., Parker, D.J., Challenor, P.G., Geake, J.E., 2005. A soft solid surface on Titan as revealed by the Huygens Surface Science Package. Nature 438, 792–795.